Frontiers of Information Technology & Electronic Engineering
www.jzus.zju.edu.cn; engineering.cae.cn; www.springerlink.com
ISSN 2095-9184 (print); ISSN 2095-9230 (online)
E-mail: jzus@zju.edu.cn

# Numerical investigation of resolution in a single emitter localization-based imaging system

Yueying WANG[1], Yiwen HU[1], Yuehan ZHAO[1], Cuifang KUANG[1,2,3], Xiang HAO[‡1,2]

[1]*College of Optical Science and Engineering, Zhejiang University, Hangzhou 310027, China*

[2]*ZJU-Hangzhou Global Science and Technological Innovation Center, Hangzhou 311100, China*

[3]*Collaborative Innovation Center of Extreme Optics, Shanxi University, Taiyuan 030006, China*

Email: yueyingw@zju.edu.cn, huyw@zju.edu.cn, zyuehan@zju.edu.cn, cfkuang@zju.edu.cn, haox@zju.edu.cn.

Received Jan. 5, 2025; Revision accepted Apr. 7, 2025; Crosschecked

Unedited

**Abstract:** In this paper, we numerically analyze the factors determining localization precision and resolution in single emitter localization-based imaging systems. While previous studies considered a limited set of parameters, our numerical approach incorporates additional parameters with significant reference value, yielding a more comprehensive analysis of the results. We differentiate between the effects of additive and multiplicative noise on localization precision using numerical modeling. Additionally, we take the influence of sampling frequency into account and compute the optimal sampling frequency for varying resolution requirements. Leveraging a suite of derived equations, we systematically simulate and quantify how variations in these parameters influence system performance. Furthermore, we provide guidelines for optimizing signal-to-noise ratio (SNR) requirements and pixel size selection based on point spread function (PSF) width in single emitter localization-based imaging systems. This numerically driven research establishes a solid foundation, offering critical insights for the analysis of more complex imaging systems.

**Key words:** localization precision; resolution; single-point positioning; oversampling; signal-to-noise ratio.
https://doi.org/10.1631/FITEE.2500015 **CLC number:**

## [1]1 Introduction

Resolution is a fundamental parameter in optical imaging systems, directly determining the amount of information a system can capture. Researchers have long focused on methods to improve it. However, resolution enhancement is constrained by the Abbe diffraction limit; when passing through the optical system, an ideal point object becomes a spot due to diffraction, meaning that two closely spaced points may become indistinguishable. Efforts have been made to break through the diffraction limit barrier using various approaches. Stimulated emission depletion microscopy (STED) (Hell and Wichmann, 1994; Bergermann *et al.*, 2015) and structured illumination microscopy (SIM) (Gustafsson, 2000; Gustafsson, 2005) have achieved improved resolution through PSF engineering and frequency domain analysis. Additionally, single-molecule localization microscopy (SMLM) (Betzig *et al.*, 2006; Rust *et al.*, 2006) sidesteps the need to resolve two points by focusing on single-point imaging. In SMLM, the center position of each individual spot can be determined with greater precision than the spot's size. The localization precision and accuracy of single-point positioning methods have been extensively studied (Thompson *et al.*, 2002; Ober *et al.*, 2004; Deschout *et al.*, 2014), providing a solid theoretical and experimental foundation for understanding the limits of spatial resolution in fluorescence microscopy. The relationship between localization precision and resolution is described by Eq. (1) (Lelek *et al.*, 2021), where $R_{\text{limit}}$ represents the resolution limit of the system and $\langle \Delta x \rangle$ denotes the localization precision.

‡ Corresponding author
© Zhejiang University Press 2025

This specific mathematical relationship is derived from the statistical derivation of the relationship between full width at half maximum (FWHM) and standard deviation, offering a method to circumvent the system's diffraction limit, enabling higher imaging resolution.

$$R_{\text{limit}} = 2\sqrt{2\ln(2)}\langle \Delta x \rangle \approx 2.35\langle \Delta x \rangle . \quad (1)$$

While the issue of localization precision has been previously discussed (Thompson *et al.*, 2002), many details are still missing, and parameters have not been considered comprehensively. Our work completes the analytical process, introduces new parameters, and addresses overlooked issues. Ultimately, we draw general conclusions and provide guidelines for selecting parameters that are critical for optimizing optical imaging systems.

## 2 Theory

Fig. 1 presents a simplified optical imaging system. The imaging process in such systems can be generalized to the following steps: light from an object (either spontaneous or illuminated) passes through an optical system and is detected by a sensor; algorithms then process the detected data to produce a recognizable image.

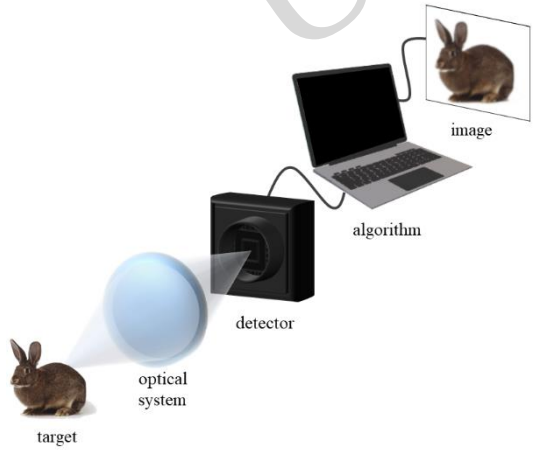


**Fig. 1. Simplified diagram of a simplified optical system**

In this simplified imaging framework, a point object is represented as an Airy spot on the detector after passing through the optical system. Typically, in an aberration-free system, a Gaussian function is used to model the Airy spot. Although the Gaussian function is symmetric, the presence of noise in actual systems prevents the direct determination of its exact center for positioning. The maximum likelihood estimation (MLE) method is widely used to calculate single-point positioning (Abraham *et al.*, 2010; Munier *et al.*, 2023) to address this issue. Starting with the fundamental shot noise, the standard deviation of the localization estimate is calculated as follows:

$$\langle (\Delta x)^2 \rangle = \frac{s^2}{N}, \quad (2)$$

where $s$ refers to the standard deviation of the Gaussian function, which is related to the full width at half maxima (FWHM) of the point spread function (PSF), and $N$ is the number of photons that reach the detector. It is evident that localization precision positively correlates with $s$ and is inversely proportional to $N$. Thus, an infinite number of photons leads to infinite localization precision.

However, several unavoidable challenges arise in the actual imaging process. The limited size of detector pixels introduces statistical errors, commonly referred to as pixelation noise (Thompson *et al.*, 2002). This error results from the statistical variance of the flat-top function, which is caused by the inability to precisely obtain the position of the photon within a finite pixel size. Additionally, quantum efficiency and the pixel filling factor reduce the number of photons that can be detected by the detector, meaning that not all photons reaching the detector are captured. Considering these points, we have (see supplementary Note 1 for the derivation):

$$\langle (\Delta x)^2 \rangle = \frac{s^2 + (p\alpha)^2/12}{N\alpha\eta}, \quad (3)$$

where $p$ is the sampling interval, which is the pixel pitch of the detector divided by the magnification of the system, equivalent to the pixel size in the raw image; $\eta$ is the quantum efficiency; and $\alpha$ is the filling factor of pixels on the detector. Considering the sampling requirements, $p$ is often chosen to be much smaller than $s$. At the same time, smaller $p$ with larger $\eta$ and $\alpha$ can directly improve the localization precision, which is also consistent with the tendency of detector selection in practice. Eq. (3) and the above deductions are valid for both one- (1D) and two-dimensional (2D) cases.

Besides shot and pixelation noise, there are other types of noise the power of which cannot be accurately described. Based on their correlation with the

Unedited

signal, they can be classified as additive noise and multiplicative noise. Additive noise mainly comprises thermal noise or other sources unrelated to the signal. The additive white Gaussian noise (AWGN) model has long been proposed and is widely adopted for analyzing the impact of additive noise on imaging (Jain, 1989). Meanwhile, multiplicative noise, directly related to the number of photons received by the detector, is often overlooked or incorporated into the analysis of additive noise (Sanches *et al.*, 2008; Merhav, 2021). Multiplicative noise is usually generated by the amplifier circuit or gain element in the system. Confusing the two noise types introduces errors into the analysis. Based on this, for 1D cases, the expected uncertainty $\sigma_i$ of the number of photons $N_i$ at $x_0$ involving both additive noise and multiplicative noise can be written as

$$\sigma_i^2 = N_i + b_1^2 + (b_2 N\alpha\eta)^2, \tag{4}$$

$$N_i = \frac{N\alpha\eta}{\sqrt{2\pi}s} e^{-\frac{i^2}{2s^2}}, \tag{5}$$

where $b_1$ represents the magnitude of additive noise, and $b_2$ represents the coefficients of multiplicative noise. The localization estimate can be calculated by

$$\langle(\Delta x)^2\rangle = \frac{1}{\sum \frac{N_i'^2}{\sigma_i^2}}, \tag{6}$$

where $N_i'$ is the derivative of $N_i$ evaluated at $x_0$. Considering the case where the signal dominates and the noise is suppressed, this equation can be incorporated into Eq. (2). In particular, if the additive noise is much greater than the number of photons, this equation can be rewritten as

$$\langle(\Delta x)^2\rangle \approx \frac{4\sqrt{\pi}s^3 b_1^2}{pN^2\alpha^2\eta^2}. \tag{7}$$

In contrast, if multiplicative noise is dominant, this equation becomes

$$\langle(\Delta x)^2\rangle \approx \frac{4\sqrt{\pi}s^3 b_2^2}{p}. \tag{8}$$

We can reach some primary conclusions from the above two equations (see supplementary Note 2 for the derivation). Larger noise leads to a decrease in the localization precision. In contrast to the pixelation noise discussed above, the larger the pixel size, the smaller the impact of background noise, and the higher the localization precision. Therefore, the whole localization uncertainty is written as Eq. (9).

$$\langle(\Delta x_{1D})^2\rangle = \frac{s^2 + (p\alpha)^2/12}{N\alpha\eta} + \frac{4\sqrt{\pi}s^3 b_1^2}{pN^2\alpha^2\eta^2} + \frac{4\sqrt{\pi}s^3 b_2^2}{p}. \tag{9}$$

The two-dimensional case can be given similarly.

$$\langle(\Delta x_{2D})^2\rangle = \frac{s^2 + (p\alpha)^2/12}{N\alpha\eta} + \frac{8\pi s^4 b_1^2}{p^2N^2\alpha^2\eta^2} + \frac{8\pi s^4 b_2^2}{p^2}. \tag{10}$$

From this, we derive the effects of additive noise, multiplicative noise, pixel pitch, and pixel filling factor on the localization precision of single points in both 1D and 2D cases. However, these results do not accord with the actual situation. When the pixel size is determined, minimizing *s* appears to improve localization precision without limit. Additionally, the localization uncertainty is smaller than the pixel size even when the FWHM of the PSF is smaller than the pixel size (see supplementary Fig. S1), which conflicts with how positioning works. This is because sampling requirements are not considered.

According to the Nyquist sampling theorem, effective sampling occurs when the sampling frequency is more than twice the frequency of the signal (Shannon, 1949). Therefore, the system requires $r>2p$ to function correctly (see supplementary Fig. S1), where *r* is the FWHM of the PSF. Eq. (12) represents the direct mathematical relationship between *r* and *s*. To maintain consistency throughout the study, we use *s* as the parameter characterizing the width of PSF in the subsequent context. To more accurately assess the effect of sampling, we must calculate a lower bound for the resolution under oversampling conditions.

$$R_{\text{oversampling}} = \frac{2}{(\rho \cdot f)^{\frac{1}{D}}}, \tag{11}$$

$$r = 2\sqrt{2\ln(2)}s, \tag{12}$$

where *D* is the spatial dimension of the detection, *f* is the factor of oversampling, and $\rho$ is the density of localization (Legant *et al.*, 2016). Specifically, in the 1D case, D=1 and $\rho = 1/p$. The factor *f* is $r/2p$ and

Unedited

is meaningful only if the system's sampling frequency is larger than the Nyquist sampling frequency. There is no oversampling when $r \le 2p$; this factor can always be 1. The threshold condition for s is expressed at $s \le 0.85p$, but for clarity and ease of understanding, we have retained $r$ in the equation. We give the total resolution as:

$$R_{\text{total}} = \sqrt{R_{\text{limit}}{}^2 + R_{\text{oversampling}}{}^2}\,. \tag{13}$$

In the 1D case, we have:

$$R_{1\text{D}} = \begin{cases} \sqrt{2.35^2\left(\dfrac{s^2+(p\alpha)^2/12}{N\alpha\eta} + \dfrac{4\sqrt{\pi}s^3 b_1{}^2}{pN^2\alpha^2\eta^2} + \dfrac{4\sqrt{\pi}s^3 b_2{}^2}{p} + \left(\dfrac{4p^2}{r}\right)^2\right)} & r > 2p \\ \sqrt{2.35^2\left(\dfrac{s^2+(p\alpha)^2/12}{N\alpha\eta} + \dfrac{4\sqrt{\pi}s^3 b_1{}^2}{pN^2\alpha^2\eta^2} + \dfrac{4\sqrt{\pi}s^3 b_2{}^2}{p} + (2p)^2\right)} & r \le 2p \end{cases}. \tag{14}$$

In the 2D case, we have

$$R_{2\text{D}} = \begin{cases} \sqrt{2.35^2\left(\dfrac{s^2+(p\alpha)^2/12}{N\alpha\eta} + \dfrac{8\pi s^4 b_1{}^2}{p^2N^2\alpha^2\eta^2} + \dfrac{8\pi s^4 b_2{}^2}{p^2}\right) + \left(\dfrac{4p^2}{r}\right)^2} & r > 2p \\ \sqrt{2.35^2\left(\dfrac{s^2+(p\alpha)^2/12}{N\alpha\eta} + \dfrac{8\pi s^4 b_1{}^2}{p^2N^2\alpha^2\eta^2} + \dfrac{8\pi s^4 b_2{}^2}{p^2}\right) + (2p)^2} & r \le 2p \end{cases}. \tag{15}$$

With sampling requirements considered, we finally derive complete expressions for the resolution. These expressions reveal that the resolution width is positively correlated with the noise factor and negatively correlated with photon count and quantum efficiency. Additionally, the effects of PSF width, pixel size, and pixel filling factor on resolution are non-monotonic, meaning that direct inferences about these parameters cannot be drawn from the expressions alone.

## 3 Results

To obtain more insightful conclusions, we conducted a quantitative analysis by controlling the variables. First, we analyzed the influence of noise on localization precision. It is well established that a deterioration in the signal-to-noise ratio (SNR) of the system degrades imaging quality. The SNR expression, including shot noise, additive noise, and multiplicative noise, is given below. Although shot noise is unavoidable, there are different proportions of additive and multiplicative noise in different systems. Distinguishing the effects of additive noise from multiplicative noise provides a guideline for addressing each differently.

$$\text{SNR} = \frac{N\alpha\eta}{\sqrt{N\alpha\eta} + \sqrt{b_1{}^2 + (b_2 N\alpha\eta)^2}}\,. \tag{16}$$

Using this SNR definition, we rewrite Eq. (14) and Eq. (15) as:

$$R_{1\text{D}} = \begin{cases} \sqrt{2.35^2\left(\dfrac{s^2+(p\alpha)^2/12}{N\alpha\eta} + \dfrac{4\sqrt{\pi}s^3}{p}\left(\dfrac{1}{\text{SNR}} - \dfrac{1}{\sqrt{N\alpha\eta}}\right)^2\right) + \left(\dfrac{4p^2}{2.35s}\right)^2} & r > 2p \\ \sqrt{2.35^2\left(\dfrac{s^2+(p\alpha)^2/12}{N\alpha\eta} + \dfrac{4\sqrt{\pi}s^3}{p}\left(\dfrac{1}{\text{SNR}} - \dfrac{1}{\sqrt{N\alpha\eta}}\right)^2\right) + (2p)^2} & r \le 2p \end{cases}, \tag{17}$$

$$R_{2\text{D}} = \begin{cases} \sqrt{2.35^2\left(\dfrac{s^2+(p\alpha)^2/12}{N\alpha\eta} + \dfrac{8\pi s^4}{p^2}\left(\dfrac{1}{\text{SNR}} - \dfrac{1}{\sqrt{N\alpha\eta}}\right)^2\right) + \left(\dfrac{4p^2}{2.35s}\right)^2} & r > 2p \\ \sqrt{2.35^2\left(\dfrac{s^2+(p\alpha)^2/12}{N\alpha\eta} + \dfrac{8\pi s^4}{p^2}\left(\dfrac{1}{\text{SNR}} - \dfrac{1}{\sqrt{N\alpha\eta}}\right)^2\right) + (2p)^2} & r \le 2p \end{cases}. \tag{18}$$

In the presence of only additive noise, the SNR of the system is approximately proportional to the square root of the number of detected photons and always increases rapidly as the number of photons

Unedited

rises. In the case of only multiplicative noise, the SNR remains positively correlated with the number of detected photons. However, as the coefficient of multiplicative noise increases, the variation of SNR with the number of photons decreases. Thus, more multiplicative noise in the system will cause the system's SNR to be less sensitive to changes in the number of detected photons.

Although SNR effectively characterizes the system's noise level, it is not sufficiently straightforward for quantitative analysis in systems where both additive and multiplicative noise are present. To analyze such systems, we selected specific noise coefficients and fixed all parameters except for photon count $N$, PSF width $s$, and pixel size $p$ for quantitative analysis (Fig. 2). As proportions of additive and multiplicative noise vary with different photon counts, we set each column to represent their different proportions when SNR is 10 at 1000 detected photons. The results show that when the power of multiplicative noise exceeds 50% of the total system noise, increasing the photon count amplifies the effect of multiplicative noise, whereas reducing the photon count enhances the effect of additive noise. In systems dominated by additive noise, increasing the pixel size or reducing the PSF width improves localization precision in most instances. This law fails when the number of detected photons is large, representing the optimal sampling ratio exists under large SNR, which we discuss below. Conversely, systems dominated by multiplicative noise are less sensitive to variations in pixel size and PSF width.

Similarly, in the 2D case, the trend of uncertainty variation with the photon count $N$ under the same coefficients of additive and multiplicative noise is consistent with the 1D case (see Supplementary Fig. S3). However, the overall uncertainty in 2D is larger than in 1D, and it is more sensitive to changes in photon count, PSF width, or pixel size.

Unedited

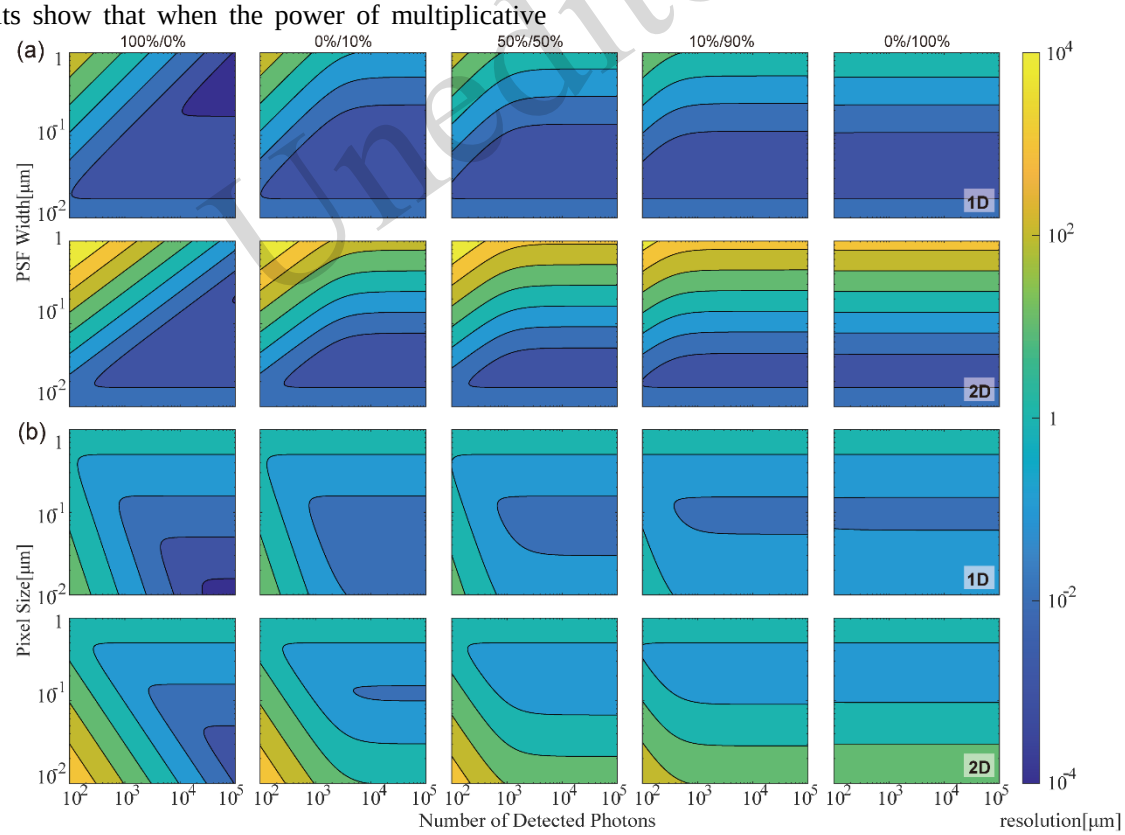


**Fig. 2. Localization precision as a function of detected photon number and PSF width (a) or pixel size (b). Each column characterizes the different proportions of additive and multiplicative noise when SNR is 10 dB at 1000 detected photons. From left to right, in each column, the proportions power of additive noise is 100%, 90%, 50%, 10%, and 0%, respectively. All results are obtained under the condition that $\alpha = 100\%$ and $\eta = 100\%$. (a) pixel size = 10 nm, (b) FWHM of PSF = 1000 nm**

This analysis enables us to draw conclusions regarding the uncertainty of the system with respect to noise. The ratio of additive to multiplicative noise in the system is variable, and increasing the number of photons may shift the dominance of multiplicative noise over additive noise. In systems dominated by additive noise, increasing photon count is the most effective strategy for reducing noise and improving performance. Conversely, in systems dominated by multiplicative noise, increasing the number of photons yields limited benefits. In such cases, reducing the PSF width or increasing pixel size can improve localization precision. Since significant adjustments to PSF width and pixel size are often impractical, these findings primarily serve as theoretical guidelines for practical experiments. While many image optimization techniques have been developed to address additive noise, multiplicative noise continues to present significant challenges. Thus, even as efforts are made to minimize the multiplicative noise figure, the influence of PSF width and pixel size should not be overlooked.

After evaluating noise, we continued to analyze the selection of PSF width *s* and pixel size *p*. These two parameters have a more complex effect on resolution than background noise, and their ratio has a more critical effect on the system's resolution than either alone. Based on Eq. (17), we selected a range of photon count *N* and SNR values to represent different illumination conditions (Fig. 3). This figure shows that SNR has a more pronounced effect on resolution than photon count *N*. As both *s* and *p* increase, the minimum resolution distance also increases. Additionally, for a fixed PSF width *s*, there exists an optimal pixel size *p* that minimizes the resolution distance. This optimal value can be determined by differentiating Eq. (17) with respect to p (see supplementary Note 3 for the derivation), and can be calculated as:

$$\begin{aligned} p &\approx 1.276s\left(\frac{1}{\mathrm{SNR}}-\frac{1}{\sqrt{N\alpha\eta}}\right)^{\frac{2}{5}} \\ &= 0.543r\left(\frac{1}{\mathrm{SNR}}-\frac{1}{\sqrt{N\alpha\eta}}\right)^{\frac{2}{5}} \end{aligned}. \tag{19}$$

Relatively, for a fixed pixel width, there is an optimal PSF width that enables the detector to achieve the best positioning effect when SNR is sufficient. This value can also be calculated as (see supplementary Note 4 for the derivation):

$$s=\frac{0.548p}{\left(\frac{1}{\mathrm{SNR}}-\frac{1}{\sqrt{N\alpha\eta}}\right)^{\frac{2}{5}}}. \tag{20}$$

These equations reveal that simply reducing the PSF width or the pixel size alone does not necessarily improve system resolution. Using a pixel size that is too small relative to the PSF width introduces excessive noise, while using a pixel size that is too large to detect a small PSF fails to achieve high resolution due to insufficient sampling. Optimal imaging performance can be achieved using Eq. (17) or Eq. (18), where neither the pixel size nor the PSF width are wasted.

Unedited

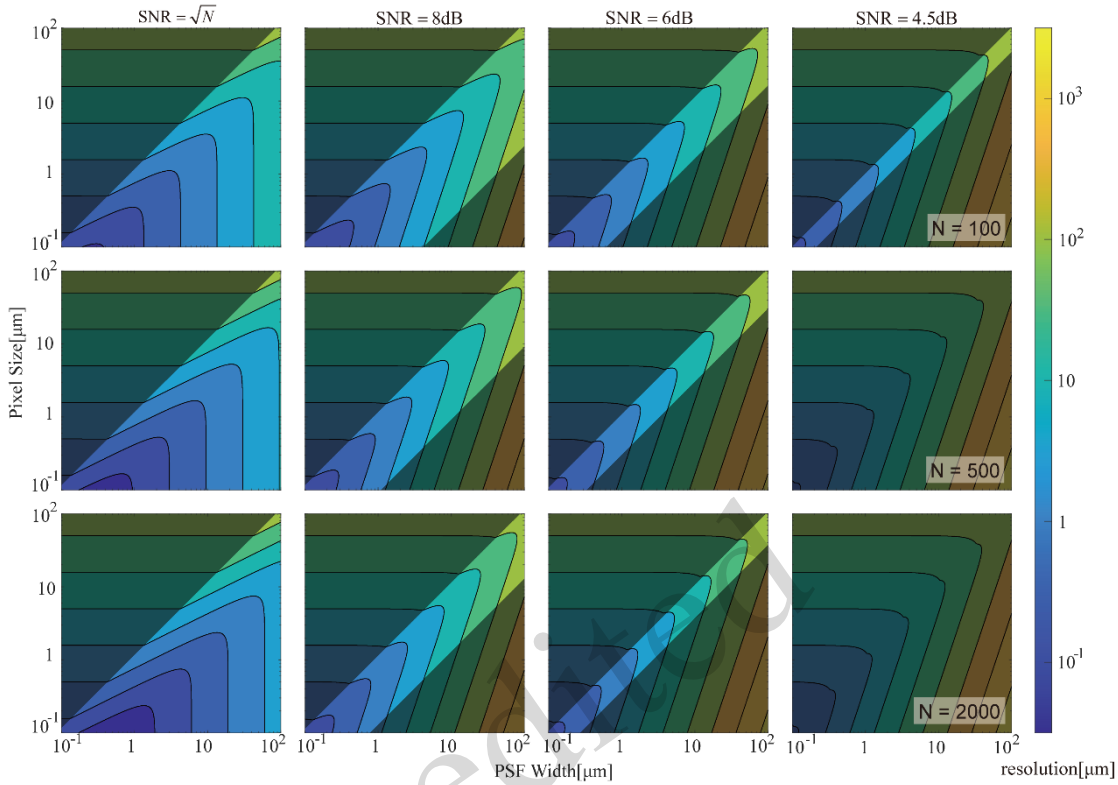


**Fig. 3. Resolution as a function of PSF width and pixel size in 1D cases. All under the condition that $\alpha = 100\%$ and $\eta = 100\%$. Each row has a different number of detected photons, and each column is under a different SNR. The SNR in the first column is exactly the square root of N, which means there is no background noise. The shaded area indicates that the resolution does not exceed the Rayleigh limit.**

Unedited

Furthermore, systems can only achieve super-resolution under well-illuminated conditions, as shown in the highlighted areas in Fig. 3. When the SNR is low or the photon count is insufficient, even if the PSF width and pixel size satisfy Eq. (19) or Eq. (20), the resulting resolution will be significantly larger than the PSF width of the system, which undermines the goal of single-point localization. The threshold SNR required to achieve higher resolution varied with the photon count. To achieve resolution beyond the Rayleigh criterion, the SNR must exceed 4.93 dB when the photon count is 1000. Additional cases with fixed SNR, photon count, or oversampling factor *f* have corresponding thresholds to achieve the expected resolution. Tables listing these thresholds are provided below. According to Eq. (19), the oversampling factor *f* should be slightly greater than 1 to achieve a resolution better than the PSF width. Eq. (21) gives a lower bound of *f* for higher resolution enhancement expectations, where *x* represents the times of resolution improvement (see supplementary Note 5 for the derivation). This condition essentially requires adherence to the Nyquist sampling law. In practice, the oversampling factor range required to meet the expected resolution depends on the SNR and photon number. Supplementary Tables 1 and 2 provide the upper and lower bounds of this range. As the photon number increases and the SNR decreases, the lower bound of the oversampling range increases while the upper bound decreases inversely. Consequently, this range narrows and eventually disappears. This result, although seemingly paradoxical, underscores the importance of carefully considering sampling conditions to achieve optimal resolution in noisier systems. Table 1 presents the minimum SNR required for different photon numbers and oversampling factor *f* to achieve a resolution better than the Rayleigh limit. The minimum SNR can be its lowest when *f* is around 1.50. Both larger and smaller oversampling ratios require an increase in the system's SNR. Therefore, setting the PSF width *s* to be three times larger than pixel size *p* can make systems

that expect a resolution to meet the Rayleigh limit better tolerant to noise. When we expect $x$ times the resolution improvement, the optimal $f$ is about $1.50\sqrt{x}$ (see supplementary Note 5 for the derivation). This optimum value is more like a recommended limit when $x$ gets larger.

$$f > \frac{1}{\sqrt[4]{\frac{1}{x^2}-\frac{1}{N}}} \approx \sqrt{x}\,. \tag{21}$$

**Table 1 Lower bound of SNR (dB) with different detected photon numbers and oversampling factor to achieve resolution beyond Rayleigh limit in 1D cases**

| Oversampling factor | Number of detected photons | | | | |
|---|---|---|---|---|---|
| | 100 | 200 | 500 | 1000 | 2000 |
| 1.05 | 5.82 | 6.28 | 6.76 | 7.02 | 7.23 |
| 1.32 | 4.11 | 4.44 | 4.76 | 4.93 | 5.05 |
| 1.5 | 4.03 | 4.35 | 4.66 | 4.83 | 4.95 |
| 2 | 4.23 | 4.58 | 4.91 | 5.08 | 5.21 |
| 3 | 4.78 | 5.18 | 5.56 | 5.77 | 5.92 |
| 5 | 5.51 | 5.98 | 6.45 | 6.71 | 6.90 |

The same is given for the 2D case (see Supplementary Fig. S4). The trends and values do not change much compared to the 1D case. However, decreasing the pixel width when the PSF width is fixed makes the slope of the iso-value line become smaller, meaning that the magnitude of the uncertainty increase increases.

$$\begin{aligned} p &\approx 0.722r\left(\frac{1}{\mathrm{SNR}}-\frac{1}{\sqrt{N\alpha\eta}}\right)^{\frac{1}{3}}, \\ &= 1.698s\left(\frac{1}{\mathrm{SNR}}-\frac{1}{\sqrt{N\alpha\eta}}\right)^{\frac{1}{3}} \end{aligned} \tag{22}$$

$$s \approx \frac{0.467p}{\left(\frac{1}{\mathrm{SNR}}-\frac{1}{\sqrt{N\alpha\eta}}\right)^{\frac{1}{3}}}\,. \tag{23}$$

The two extrema are calculated using the same method. Compared to the 1D case, the optimal pixel size for the same PSF width is larger. The range of alternative sampling rates under different SNR and photon numbers varies in the same way as in 1D cases (see Supplementary Tables 3 and 4). Table 2 presents the minimum SNR required for different photon numbers and oversampling factor $f$ to achieve a resolution better than the PSF width. The optimal oversampling factor changes to $1.32\sqrt{x}$ (see Supplementary Note 5). The SNR required to achieve comparable resolution is significantly higher than in the 1D case. Additionally, as the number of photons increases, the required minimum SNR rises more rapidly, indicating that 2D situations are more sensitive to noise.

**Table 2 Lower bound of SNR (dB) with different detected photon numbers and over-sampling factor to achieve resolution beyond Rayleigh limit in 2D cases.**

| Oversampling factor | Number of detected photons | | | | |
|---|---|---|---|---|---|
| | 100 | 200 | 500 | 1000 | 2000 |
| 1.05 | 7.19 | 7.87 | 8.60 | 9.02 | 9.35 |
| 1.32 | 6.12 | 6.66 | 7.21 | 7.52 | 7.75 |
| 1.5 | 6.22 | 6.77 | 7.34 | 7.66 | 7.90 |
| 2 | 6.72 | 7.35 | 8.01 | 8.39 | 8.67 |
| 3 | 7.51 | 8.29 | 9.13 | 9.62 | 10.00 |
| 5 | 8.34 | 9.30 | 10.39 | 11.05 | 11.60 |

Here, we provide guidance on selecting the optimal PSF-width-to-pixel-size ratio based on sampling requirements in both 1D and 2D systems: for optimal imaging resolution, these two parameters

Unedited

must be matched to balance the effects of noise and sampling. Once other parameters are determined, the optimal value for the remainder can be calculated using Eq. (19) and Eq. (20) (or, in the case of 2D, Eq. (22) and Eq. (23)). Additionally, thresholds for achieving super-resolution are presented in the tables above and in the supplementary material. However, in a specific system, both PSF width and pixel size are influenced by other optical parameters that are not addressed in this discussion. PSF width depends on the system's wavelength and numerical aperture, while pixel size is determined by the detector pixel pitch divided by the magnification of the system. These parameters cannot be adjusted arbitrarily, and some are interrelated, such as numerical aperture and magnification. Furthermore, for specific imaging targets, these parameters may be constrained by factors beyond imaging performance. For instance, in fluorescence imaging systems, the wavelength must match the dye's spectrum and cannot be freely changed. Therefore, optimizing system parameter selection by combining application requirements with imaging conditions is essential to achieve the best possible system performance.

Finally, we consider the detector's quantum efficiency and pixel-filling factor. The influence of these two parameters on localization precision is relatively straightforward. Quantum efficiency impacts only the number of detected photons, making it critical to select a detector with the highest possible quantum efficiency. The pixel-filling factor affects the effective pixel area, which accounts for the number of photons detected. Although increasing the effective detection area will introduce more pixelation noise, this effect is negligible compared to the uncertainty caused by a reduction in the number of detected photons. Pixelation noise becomes significant only when the pixel size is several times larger than the PSF width. In such cases, a conclusion can be drawn by analyzing the previously derived equations. Therefore, maximizing both the pixel-filling factor and the quantum efficiency is recommended to optimize performance.

## 4 Discussion

In this paper, we have provided detailed equations on the localization precision and resolution of single-point positioning systems. The parameters discussed reflect the basic performance of the optical system and detector. To reach general conclusions with practical guidance, we have simplified several issues, and some parameters were not introduced. Instead, our conclusion stems from specific condition constraints. It may introduce specific variables into our formulations for more targeted analyses of specific cases.

First, we adopted the Gaussian function to model the PSF distribution, but our theoretical framework is not constrained to this choice. In practice, the actual PSF distribution may be Bessel or another form that may not fit a standard function (Janssen, 2002; Legant *et al.*, 2016). In such cases, numerical integration incorporating the experimentally determined PSF can be substituted for Eq. (5). The Gaussian function used in this study serves as a representative model that yields instructive theoretical insights.

Aberrations were not included in our discussions. Many systems incorporate aberration correction, and the results can often be interpreted as aberration-free (Snoeyink, 2013; Virant *et al.*, 2017). However, in systems with aberrations, multiple aberrations may be present, making it challenging to derive general conclusions (Tachi *et al.*, 2021). For example, spherical aberration can be seen as a superposition of PSF broadening and multiplicative noise (Deng and Shaevitz, 2009). Numerical integration of the actual PSF distribution can reflect spherical aberration to some extent. However, aberrations like coma lead to asymmetrical PSF distributions, resulting in incorrect single-point positioning. Additionally, the points at different positions on the imaging plane show different PSF distributions and localization precision due to aberration (Hughes *et al.*, 2023). The analysis of the influence of aberrations on the positioning uncertainty is of no general application value. In practice, it is more necessary to eliminate the influence of aberration as much as possible through the adjustment of the optical design (Deng and Shaevitz, 2009; Izeddin *et al.*, 2012) or the correction of the algorithm (Liu *et al.*, 2024). Thus, this paper does not delve into the effects of aberrations on localization precision, though this could be explored further based on our work. For certain unavoidable aberrations, their effects on localization precision can be quantitatively analyzed by incorporating the aberration-distorted PSF into our theoretical framework.

Unedited

System instabilities, such as sample drift and temperature fluctuations, which affect detection accuracy rather than precision, are also beyond the scope of this discussion.

Regarding detectors, we did not specify a particular type in this study. However, our conclusions are applicable across a broad range of detectors for single-point positioning. CCD, CMOS, and any other systems that rely on photon detection at the pixel level can do. However, there are several important parameters that we did not account for, which can affect detector performance. For instance, dark counts which is the false detection of photons in the absence of light, can introduce noise and reduce overall signal quality. Similarly, readout noise that generated during the conversion of the detected photons into an electrical signal,can further degrade the quality of the output image. These noise factors, if unaddressed, can cause discrepancies between the actual number of photons detected and the true photon count from the optical system, thereby skewing the results. Another potential limitation arises from detectors in which the electrical signal is not linearly related to the number of photons received (Křížek *et al.*, 2011). Nonlinearity in the detector response can lead to distortions of PSF distribution, complicating the accurate estimation of localization precision. In cases where nonlinearity is significant, advanced calibration techniques may be required to mitigate these effects.

Discussion is limited to the 2D case, and the 3D case has not been explored, primarily because fully developed volumetric detectors are not yet available. Most existing 3D imaging methods rely on axial slicing (Chen *et al.*, 2014) or computational methods that reconstruct 3D volumes from 2D imaging data (Yu *et al.*, 2016; von Diezmann *et al.*, 2017). In both methods, the precision of 3D positioning is heavily dependent on the resolution and precision of the underlying 2D imaging system. In addition, 3D reconstruction algorithms introduce further uncertainties due to the mathematical models and assumptions used, complicating the process.

Post-processing of the electrical signal is another critical factor that can significantly influence localization precision. Once the raw data are collected by the detector, they typically undergo post-processing algorithms aimed at refining the signal, reducing noise, and correcting distortions introduced during detection. These algorithms, such as noise reduction techniques (Wolter *et al.*, 2010), deconvolution (Mukamel *et al.*, 2012), and image reconstruction (Liu *et al.*, 2020; Liu *et al.*, 2024), can play a crucial role in enhancing the final resolution and accuracy of the imaging system. For example, deconvolution algorithms are frequently used to reverse the blurring effects introduced by the optical system, leading to sharper images and more precise localization. While effective post-processing can greatly improve localization precision, it also introduces additional complexities, such as the risk of introducing artifacts or biasing the final image if improperly applied. Our study, however, primarily focuses on the performance at the detector level, examining the inherent limitations and characteristics of the detector itself without delving into the complexities of post-processing. The influence of post-processing algorithms, while important, falls outside the scope of our current analysis. Future work could expand on this by incorporating post-processing techniques to evaluate how they interact with the detector's raw data and contribute to the overall system's localization precision and resolution.

Additionally, the localization precision analysis algorithm presented in this paper is primarily a theoretical tool designed to assist researchers in evaluating the impact of system parameter choices on final results before conducting experiments. To analyze specific experimental data, our algorithm is mainly applied to data reconstruction rather than as a definitive measure of final resolution. To assess the resolution of specific experimental outcomes, frequency-domain methods, such as Fourier ring correlation (FRC) (Banterle *et al.*, 2013), provide greater convenience and broader applicability.

In conclusion, our work provides guidelines for assessing localization precision and resolution in most optical systems for single-point imaging. The effects of background noise and sampling frequency are analyzed in detail. The model presented is fundamental and detailed, allowing for general conclusions. Further complexity can be introduced by refining the calculations, such as substituting the PSF distribution in our equations. Additionally, our discussion does not limit the system's operating wavelength, making these conclusions relevant for imaging in other electromagnetic wavebands with similar

Unedited

propagation characteristics.

## Contributors

Yueying WANG conceptualized and designed the study, conducted formal analysis, developed the software, validated the results, and finalized the paper. Yiwen HU contributed to software development and critically revised the paper. Yuehan ZHAO was responsible for validation procedures. Cuifang KUANG contributed to the conceptualization and secured funding for the project. Xiang HAO led the conceptualization, secured funding, and revised the paper.

## Conflict of interest

All the authors declare that they have no conficts of interest.

## Data availability

The data that support the findings of this study are available from the corresponding author upon reasonable request.

## References

Abraham AV, Ram S, Chao J, et al., 2010. Comparison of estimation algorithms in single-molecule localization. Three-Dimensional and Multidimensional Microscopy: Image Acquisition and Processing XVII, p.28-34. https://doi.org/10.1117/12.842178

Banterle N, Bui KH, Lemke EA, et al., 2013. Fourier ring correlation as a resolution criterion for super-resolution microscopy. *J Struct Biol*, 183(3):363-367. https://doi.org/10.1016/j.jsb.2013.05.004

Bergermann F, Alber L, Sahl SJ, et al., 2015. 2000-fold parallelized dual-color STED fluorescence nanoscopy. *Opt Express*, 23(1):211-223. https://doi.org/10.1364/OE.23.000211

Betzig E, Patterson GH, Sougrat R, et al., 2006. Imaging intracellular fluorescent proteins at nanometer resolution. *Science*, 313(5793):1642-1645. https://doi.org/10.1126/science.1127344

Chen BC, Legant WR, Wang K, et al., 2014. Lattice light-sheet microscopy: imaging molecules to embryos at high spatiotemporal resolution. *Science*, 346(6208):1257998. https://doi.org/10.1126/science.1257998

Deng Y, Shaevitz JW, 2009. Effect of aberration on height calibration in three-dimensional localization-based microscopy and particle tracking. *Appl Opt*, 48(10): 1886-1890. https://doi.org/10.1364/AO.48.001886

Deschout H, Zanacchi FC, Mlodzianoski M, et al., 2014. Precisely and accurately localizing single emitters in fluorescence microscopy. *Nat Methods*, 11(3):253-266. https://doi.org/10.1038/nmeth.2843

Gustafsson MGL, 2000. Surpassing the lateral resolution limit by a factor of two using structured illumination microscopy. *J Microsc*, 198(2):82-87. https://doi.org/10.1046/j.1365-2818.2000.00710.x

Gustafsson MGL, 2005. Nonlinear structured-illumination microscopy: wide-field fluorescence imaging with theoretically unlimited resolution. *Proc Natl Acad Sci USA*, 102(37):13081-13086. https://doi.org/10.1073/pnas.0406877102

Hell SW, Wichmann J, 1994. Breaking the diffraction resolution limit by stimulated emission: stimulated-emission-depletion fluorescence microscopy. *Opt Lett*, 19(11):780-782. https://doi.org/10.1364/OL.19.000780

Hughes JM, DeForest CE, Seaton DB, 2023. Coma off it: regularizing variable point-spread functions. *Astron J*, 165(5):204. https://doi.org/10.3847/1538-3881/acc578

Izeddin I, El Beheiry M, Andilla J, et al., 2012. PSF shaping using adaptive optics for three-dimensional single-molecule super-resolution imaging and tracking. *Opt Express*, 20(5):4957-4967. https://doi.org/10.1364/OE.20.004957

Jain A, 1989. Fundamentals of Digital Image Processing. Prentice Hall, Englewood Cliffs, USA.

Janssen AJEM, 2002. Extended Nijboer–Zernike approach for the computation of optical point-spread functions. *J Opt Soc Am A*, 19(5):849-857. https://doi.org/10.1364/JOSAA.19.000849

Křížek P, Raška I, Hagen GM, 2011. Minimizing detection errors in single molecule localization microscopy. *Opt Express*, 19(4):3226-3235. https://doi.org/10.1364/OE.19.003226

Legant WR, Shao L, Grimm JB, et al., 2016. High-density three-dimensional localization microscopy across large volumes. *Nat Methods*, 13(4):359-365. https://doi.org/10.1038/nmeth.3797

Lelek M, Gyparaki MT, Beliu G, et al., 2021. Single-molecule localization microscopy. *Nat Rev Methods Primers*, 1(1):39. https://doi.org/10.1038/s43586-021-00038-x

Liu S, Chen JW, Hellgoth J, et al., 2024. Universal inverse modeling of point spread functions for SMLM localization and microscope characterization. *Nat Methods*, 21(6):1082-1093. https://doi.org/10.1038/s41592-024-02282-x

Liu X, Tu SJ, Xu Y, et al., 2020. Aberrations in structured illumination microscopy: a theoretical analysis. *Front Phys*, 7:254. https://doi.org/10.3389/fphy.2019.00254

Merhav N, 2021. Optimal correlators for detection and estimation in optical receivers. *IEEE Trans Inform Theory*, 67(8):5200-5210. https://doi.org/10.1109/TIT.2021.3089593

Mukamel EA, Babcock H, Zhuang XW, 2012. Statistical deconvolution for superresolution fluorescence microscopy. *Biophys J*, 102(10):2391-2400. https://doi.org/10.1016/j.bpj.2012.03.070

Munier N, Soubies E, Weiss P, 2024. The MLE is a reliable

Unedited

source: sharp performance guarantees for localization problems. *Inverse Problems*, 40(1):014001. https://doi.org/10.1088/1361-6420/ad0dbb

Ober RJ, Ram S, Ward ES, 2004. Localization accuracy in single-molecule microscopy. *Biophys J*, 86(2):1185-1200. https://doi.org/10.1016/S0006-3495(04)74193-4

Rust MJ, Bates M, Zhuang XW, 2006. Sub-diffraction-limit imaging by stochastic optical reconstruction microscopy (STORM). *Nat Methods*, 3(10):793-796. https://doi.org/10.1038/nmeth929

Sanches JM, Nascimento JC, Marques JS, 2008. Medical image noise reduction using the sylvester–lyapunov equation. *IEEE Trans Image Process*, 17(9):1522-1539. https://doi.org/10.1109/TIP.2008.2001398

Shannon CE, 1949. Communication in the presence of noise. *Proc IRE*, 37(1):10-21. https://doi.org/10.1109/JRPROC.1949.232969

Snoeyink C, 2013. Imaging performance of Bessel beam microscopy. *Opt Lett*, 38(14):2550-2553. https://doi.org/10.1364/OL.38.002550

Tachi K, Hirasawa T, Okawa S, et al., 2021. Chromatic-aberration-free multispectral optical-resolution photoacoustic microscopy using reflective optics and a supercontinuum light source. *Appl Opt*, 60(31):9651-9658. https://doi.org/10.1364/AO.434817

Thompson RE, Larson DR, Webb WW, 2002. Precise nanometer localization analysis for individual fluorescent probes. *Biophys J*, 82(5):2775-2783. https://doi.org/10.1016/S0006-3495(02)75618-X

Virant D, Turkowyd B, Balinovic A, et al., 2017. Combining primed photoconversion and UV-photoactivation for aberration-free, live-cell compliant multi-color single-molecule localization microscopy imaging. *Int J Mol Sci*, 18(7):1524. https://doi.org/10.3390/ijms18071524

von Diezmann L, Shechtman Y, Moerner WE, 2017. Three-dimensional localization of single molecules for super-resolution imaging and single-particle tracking. *Chem Rev*, 117(11):7244-7275. https://doi.org/10.1021/acs.chemrev.6b00629

Wolter S, Schüttpelz M, Tscherepanow M, et al., 2010. Real-time computation of subdiffraction-resolution fluorescence images. *J Microsc*, 237(1):12-22. https://doi.org/10.1111/j.1365-2818.2009.03287.x

Yu B, Yu J, Li WH, et al., 2016. Nanoscale three-dimensional single particle tracking by light-sheet-based double-helix point spread function microscopy. *Appl Opt*, 55(3):449-453. https://doi.org/10.1364/AO.55.000449

Unedited